EXTENDED OBJECT TRACKING USING HIERARCHICAL TRUNCATION MEASUREMENT MODEL WITH AUTOMOTIVE RADAR

Y. Xia, P. Wang, K. Berntorp, T. Koike-Akino, H. Mansour, M. Pajovic, P. Boufounos, and P. V. Orlik*

Mitsubishi Electric Research Laboratories (MERL), Cambridge, MA 02139, USA

ABSTRACT

Motivated by real-world automotive radar measurements that are distributed around object (e.g., vehicles) edges with a certain volume, a novel hierarchical truncated Gaussian measurement model is proposed to resemble the underlying spatial distribution of radar measurements. With the proposed measurement model, a modified random matrix-based extended object tracking algorithm is developed to estimate both kinematic and extent states. In particular, a new state update step and an online bound estimation step are proposed with the introduction of pseudo measurements. The effectiveness of the proposed algorithm is verified in simulations.

***Index Terms*—** Automotive radar, Bayesian filtering, object tracking, extended object, random matrix, autonomous driving.

1. INTRODUCTION

Autonomous driving has received increasing attention over the past few years. Automotive radar, along with ultrasonic, camera and LIDAR sensors, is an indispensable component, providing reliable environmental perception in all-weather conditions, with affordable cost. In this paper we focus on object tracking using automotive radar measurements. Within this context, we explore extended object tracking (EOT) which uses multiple measurements per object to improve tracking capability, exploiting an augmented state description including object kinematics and extent, compared to traditional point object tracking of a kinematic-only state [1–8].

Our approach uses a Bayesian filtering framework, which benefits from a probabilistic measurement model to describe multiple measurements per object given the object state (e.g., position, kinematic, and extent). Such probabilistic models capture both the *spatial model*, i.e., how radar measurements are spatially distributed around the object, and the characteristics of sensor noise. In contrast, early work uses a *fixed set of points* to model a rigid body and requiring a non-scalable data association between those points and radar measurements [9–11].

Our approach follows the paradigm of recent work on flexible spatial models. In this framework, automotive radar measurements are spatially distributed as a function of individual measurement likelihoods, also referred to as the spatial distribution. For automotive radar measurements, the spatial distribution can be generally divided into the three categories shown in Fig. 1: (a) contour models that reflect the measurement distribution along the contour [12, 13]; (b) surface models that assume the radar measurements are generated from the inner surface of objects; and (c) surface-volume models that balance between the above models with more realistic features, such as low measurement likelihood at the center.

*Yuxuan Xia is a PhD student at Chalmers University of Technology, Gothenburg, Sweden. This work was done during his internship at MERL.

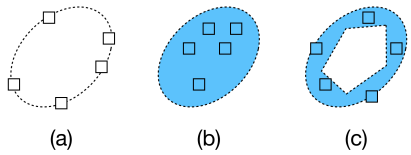

Fig. 1: Spatial distributions for automotive radar measurements: a) contour model; b) surface model; and c) surface-volume model.

Typical examples of the contour model include a rectangular shape model around four edges [14, 15] and a curve approximation using Gaussian process [16, 17]. A widely used surface model is the elliptical object shape where a random matrix is used to track extended objects [18, 19]. The surface model often leads to computationally simpler algorithms than the contour model, which requires more degrees of freedom to describe more complex shapes.

However, real-world automotive radar measurements are typically distributed around edges of rigid objects (e.g., vehicles) with a certain volume, see [20, Fig. 1] and [21, Fig. 3]. This motivates recent developments of surface-volume models including a volcanormal measurement model [20] that pushes the measurement likelihood away from its center, and a completely data-driven measurement model that is trained offline by aggregating real-world automotive radar measurements using a variational Gaussian mixture [21].

In this paper, we propose a new surface-volume model to resemble the spatial distributional characteristics of real-world automotive radar measurements. This is achieved by introducing a hierarchical truncated Gaussian measurement model where unobserved measurement sources are used to capture the feature that radar measurements are more likely to appear around object edges with a certain volume. The observable noisy measurements, conditioned on the measurement sources, are used to model sensor noise.

To integrate the proposed model into the Bayesian filtering framework, we develop a new measurement update step within the random matrix model of [19] using pseudo measurements and the resulting converted measurement statistics. In addition, we treat the truncation bounds of the truncated Gaussian distribution as unknown parameters and introduce an online estimation step to adaptively update them, for a more accurate spatial distribution.

2. PROBLEM FORMULATION

We define the object state as a tuple $\xi_k = (x_k, X_k)$ with $x_k \in \mathbb{R}^{d_x}$ denoting the *kinematic* state and $X_k \in \mathbb{S}^2_{++}$, a symmetric and positive definite matrix, denoting the *extent* state. For each time step k, we receive n_k measurements $Z_k \triangleq \{z_k^j\}_{j=1}^{n_k}$ from automotive radar sensors. The objective of object tracking is to recursively compute the posterior density of the object state $p(\xi_k|Z_{1:k})$ given all measurements $Z_{1:k} = \{Z_1, \cdots, Z_k\}$ up to and including time k. The object state ξ_k with corresponding uncertainty measures can then be

extracted from the posterior density $p(\xi_k|Z_{1:k})$.

Recursive Bayesian filtering assumes the posterior density $p(\xi_{k-1}|Z_{1:k-1})$ at time $k-1$ and the transition density $p(\xi_k|\xi_{k-1})$. First, a predicted density is derived from the Chapman-Kolmogorov equation (state prediction)

$$p(\xi_k|Z_{1:k-1}) = \int p(\xi_{k-1}|Z_{1:k-1})p(\xi_k|\xi_{k-1})d\xi_{k-1}. \quad (1)$$

This density is then updated (state update) with the current measurements Z_k as

$$p(\xi_k|Z_{1:k}) \propto p(\xi_k|Z_{1:k-1})p(Z_k|\xi_k), \quad (2)$$

where $p(Z_k|\xi_k) = \prod_{j=1}^{n_k} p(z_k^j|\xi_k)$ is the joint measurement likelihood with $p(z_k^j|\xi_k)$ denoting the spatial distribution. We approximate the predicted and posterior state densities such that they are all of the same functional form, which allows a recursive use of the prediction and update functions.

3. PROPOSED MEASUREMENT MODEL

To capture the spatial characteristics of automotive radar measurements, we propose a hierarchical measurement model for the spatial distribution $p(z_k^j|\xi_k)$. Specifically, we model each measurement z_k^j as $z_k^j = y_k^j + v_k^j$. The noisy measurement conditioned on the measurement source $p(z_k^j|y_k^j)$ is modeled using the Gaussian distribution $\mathcal{N}(z_k^j; y_k^j, R_k)$ with R_k denoting the measurement noise covariance matrix and the corresponding hidden *measurement source* y_k^j is distributed as

$$\mathcal{TN}(y_k^j; Hx_k, \rho X_k, D_k) = \frac{\mathbf{1}_{D_k}(y_k^j)}{c_{D_k}} \mathcal{N}(y_k^j; Hx_k, \rho X_k), \quad (3)$$

where H is the observation matrix, ρ is a scaling factor, D_k specifies the truncated Gaussian density support, $\mathbf{1}_{D_k}(\cdot)$ is the indicator function on D_k, and c_{D_k} is the corresponding normalization factor. An illustrative example for the measurement source y_k^j is shown in the top plot of Fig. 2. The truncated area is described by $B_k \triangleq [a_{k,1}, a_{k,2}, b_{k,1}, b_{k,2}]^T$ with respect to the object center Hx_k. It requires that $\{a_{k,1}, a_{k,2}, b_{k,1}, b_{k,2}\} \geq 0$ and that the orientation of the truncated area is aligned with the object's orientation.

Given the hierarchical measurement model above, the resulting spatial distribution $p(z_k^j|\xi_k)$ can be computed by marginalizing out the measurement source y_k^j

$$\begin{aligned} p(z_k^j|\xi_k) &= \int p(z_k^j|y_k^j)p(y_k^j|\xi_k)dy_k^j \\ &= \frac{1}{c_{D_k}} \int_{D_k} \mathcal{N}(z_k^j; y_k^j, R_k)\mathcal{N}(y_k^j; Hx_k, \rho X_k)dy_k^j. \end{aligned} \quad (4)$$

An illustration of $p(z_k^j|\xi_k)$ is shown in the bottom plot of Fig. 2. As shown, the proposed hierarchical measurement model pushes the measurement likelihood away from the object center onto four edges, which enables a better resemblance to the distribution of real-world automotive radar measurements. It is worth noting that the proposed hierarchical measurement model can also be used to describe partially observed radar measurements due to self-occlusion, e.g., when only the rear part of a vehicle is observable, by setting one or more truncation bounds to infinity.

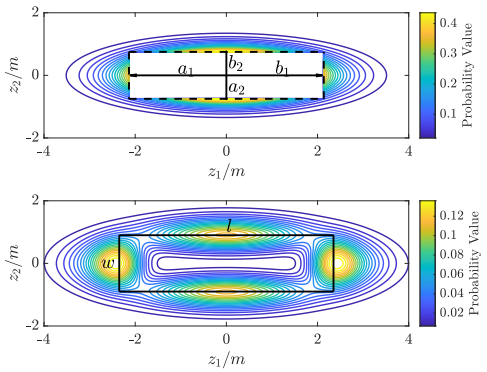

Fig. 2: Top: the probability density of the measurement source $p(y_k^j|\xi_k)$ of (3) centered at the origin of coordinates ($\rho = 0.25$, $l = 4.7$, $w = 1.8$, $a_1 = b_1 = 2.14$ and $a_2 = b_2 = 0.75$). Bottom: the resulting spatial distribution $p(z_k^j|\xi_k)$ of (4) with $R_k = \text{diag}([0.09, 0.09])$.

4. PROPOSED EOT ALGORITHM

Using the proposed measurement model, we propose to estimate the object state ξ_k and the truncation bounds B_k by iterating a two-step procedure until a convergence criterion is met. In the t-th iteration, we first use the filtered state estimates $\xi_k^{(t-1)}$ from the previous iteration to update the truncation bounds $B_k^{(t)}$ from the maximum likelihood estimation. Then, we introduce a modified random matrix-based EOT algorithm [19] with $B_k^{(t)}$ to obtain updated state estimates $\xi_k^{(t)}$. When $t = 0$, i.e., at the first iteration, we replace the filtered state estimate $\xi_k^{(0)}$ by the predicted state estimates, i.e., $\xi_k^{(0)} = \xi_{k-1}$ from the previous time step $k-1$.

To start, we assume that both the predicted and updated state densities have the factorized form [19]

$$\begin{aligned} p(\xi_k|Z_{1:k'}) &\approx p(x_k|Z_{1:k'})p(X_k|Z_{1:k'}) \\ &= \mathcal{N}(x_k; m_{k|k'}, P_{k|k'})\mathcal{IW}(X_k; \nu_{k|k'}, V_{k|k'}), \end{aligned} \quad (5)$$

where $k' = k-1$ is for the state prediction and $k' = k$ for the state update. The kinematic state x_k is Gaussian distributed with predict/update mean $m_{k|k'}$ and covariance matrix $P_{k|k'}$, whereas the extent matrix X_k is inverse Wishart distributed with $\nu_{k|k'}$ degrees of freedom and the scale matrix $V_{k|k'}$. This factorized form allows for the modeling of non-linear dynamics [19]. Using the factorized state density, we compute $\{m, P, v, V\}_{k|k-1}$ for the state prediction and $\{m, P, v, V\}_{k|k}$ for the state update.

4.1. State Prediction

To do so, we assume the state transition density is approximated as a product of Gaussian and Wishart distributions [18]

$$\begin{aligned} &p(\xi_k|\xi_{k-1}) \approx p(x_k|x_{k-1})p(X_k|X_{k-1}, x_{k-1}) = \\ &\mathcal{N}(x_k; g(x_{k-1}), Q_{k-1})\mathcal{W}\left(X_k; \kappa_{k-1}, \frac{E_{x_{k-1}} X_{k-1} E_{x_{k-1}}^T}{\kappa_{k-1}}\right), \end{aligned} \quad (6)$$

where $g(\cdot)$ denotes a kinematic state motion model, Q_{k-1} denotes the process noise covariance and E_x denotes the transformation matrix—typically an identity matrix or a rotation matrix depending on x_{k-1}. Given the state transition density above and the

posterior density $p(\xi_{k-1}|Z_{1:k-1})$ in (5), the predicted parameters $\{m, P, v, V\}_{k|k-1}$ of $p(\xi_k|Z_{1:k-1})$ can be (approximately) calculated as [19]

$$m_{k|k-1} = g(m_{k-1|k-1}), \quad G_{k-1} = \nabla_x g(x)|_{x=m_{k-1|k-1}}, \tag{7a}$$

$$P_{k|k-1} = G_{k-1} P_{k-1|k-1} G_{k-1}^T + Q_{k-1}, \tag{7b}$$

$$\nu_{k|k-1} = 6 + e^{-T_s/\tau}(\nu_{k-1|k-1} - 6), \tag{7c}$$

$$V_{k|k-1} = e^{-T_s/\tau} E_{m_{k-1}} V_{k-1|k-1} E_{m_{k-1}}^T, \tag{7d}$$

where T_s is the sampling time and τ is a maneuvering correlation constant. The kinematic state prediction in (7a) and (7b) follows the standard prediction step of a (nonlinear) Kalman filter, whereas the extent state prediction is given by (7c) and (7d). More general extent prediction steps can be obtained by analytically solving the Chapman-Kolmogorov equation [22].

4.2. State Update

Due to the "surface-volume" characteristics of radar measurements, a direct state update with the random matrix-based approach, using the sample mean and spread is likely to yield biased state estimates. To correct such biases, we introduce a set of pseudo measurements and make use of the resulting converted measurement statistics.

Given n_k observable noisy measurements $Z_k = \{z_k^j\}_{j=1}^{n_k}$, corresponding measurement sources $Y_k \triangleq \{y_k^j\}_{j=1}^{n_k}$ are distributed according to $\prod_{j=1}^{n_k} \mathcal{TN}(y_k^j; Hx_k, \rho X_k, D_k)$. Supposing that we have n_k^c *pseudo* noisy measurements $\tilde{Z}_k \triangleq \{\tilde{z}_k^j\}_{j=1}^{n_k^c}$, independently drawn from the measurement likelihood

$$p(\tilde{z}_k^j|\xi_k) = \frac{1}{1 - c_{D_k}} \int_{D_k^c} \mathcal{N}(\tilde{z}_k^j; \tilde{y}_k^j, R_k) \mathcal{N}(\tilde{y}_k^j; Hx_k, \rho X_k) d\tilde{y}_k^j, \tag{8}$$

where corresponding *pseudo* measurement sources $\tilde{Y}_k \triangleq \{\tilde{y}_k^j\}_{j=1}^{n_k^c}$ are independently drawn from $\mathcal{TN}(\tilde{y}_k^j; Hx_k, \rho X_k, D_k^c)$ and $D_k^c = \mathbb{R}^2 \setminus D_k$, then the joint measurement sources $\breve{Y}_k = \{Y_k, \tilde{Y}_k\}$ can be regarded as equivalent samples from the Gaussian distribution $\mathcal{N}(\breve{y}_k^j; Hx_k, \rho X_k)$ when the ratio of numbers of observable and pseudo measurement satistifies

$$n_k / n_k^c = c_{D_k} / (1 - c_{D_k}). \tag{9}$$

See Fig. 4 for an illustration. It follows that the corresponding joint measurements $\breve{Z}_k = \{Z_k, \tilde{Z}_k\}$ can be regarded as equivalent samples from the distribution $\mathcal{N}(\breve{z}_k^j; Hx_k, \rho X_k + R_k)$.

The converted sample mean and spread of $\breve{Z}_k$ can be, respectively, expressed as functions of the sample mean and spread of observable measurements Z_k and pseudo measurements $\tilde{Z}_k$

$$\overline{\breve{z}}_k = \sum_{j=1}^{n_k + n_k^c} \breve{z}_k^j / (n_k + n_k^c) = c_{D_k} \overline{z}_k + (1 - c_{D_k}) \overline{\tilde{z}}_k, \tag{10a}$$

$$\Sigma_{\breve{Z}_k} = \sum_{j=1}^{n_k + n_k^c} (\breve{z}^j - \overline{\breve{z}}_k)(\breve{z}^j - \overline{\breve{z}}_k)^T. \tag{10b}$$

The pseudo measurement $\tilde{z}_k^j$ can be drawn from $\mathcal{N}(\tilde{z}_k^j; \tilde{y}_k^j, R_k)$, and the corresponding measurement source $\tilde{y}_k^j$ can be drawn from $\mathcal{TN}(\tilde{y}_k^j; Hx_{k|k}^{(t-1)}, \rho X_{k|k}^{(t-1)}, D_k^{c,(t-1)})$ where $x_{k|k}^{(t-1)}$ and $X_{k|k}^{(t-1)}$ are from the previous iteration $(t-1)$. We may replace $\sum \tilde{z}_k^j$ and $\sum \tilde{z}_k^j \{\tilde{z}_k^j\}^T$ by its expectation $\mathbb{E}\{\tilde{z}_k^j\}$ and its second-order moment $\mathbb{E}\{\tilde{z}_k^j \{\tilde{z}_k^j\}^T\}$ to avoid the pseudo-sample drawing step.

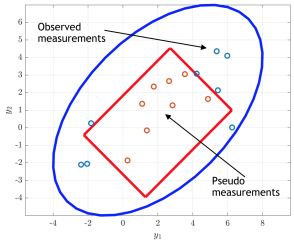

Fig. 3: The ratio between the numbers of observed (blue dots) and pseudo (red dots) measurement sources is determined by the normalization factor of the truncated Gaussian distribution.

Given the proposed measurement model (4) and the predicted density $p(\xi_k|Z_{1:k-1})$ of the form (5), the updated parameters $\{m, P, v, V\}_{k|k}$ for the updated density $p(\xi_k|Z_k)$ are given as [19]

$$m_{k|k} = m_{k|k-1} + K\varepsilon, \tag{11a}$$

$$P_{k|k} = P_{k|k-1} - KHP_{k|k-1}, \tag{11b}$$

$$\nu_{k|k} = \nu_{k|k-1} + (n_k + n_k^c), \tag{11c}$$

$$V_{k|k} = V_{k|k-1} + \hat{N} + \hat{Z}, \tag{11d}$$

where $K = P_{k|k-1} H S^{-1}$, $S = HP_{k|k-1}H^T + \hat{R}/(n_k + n_k^c)$, $\hat{R} = \rho\hat{X} + R_k$, $\hat{X} = V_{k|k-1}/(V_{k|k-1} - 6)$ and $\varepsilon = \overline{\tilde{z}}_k - Hm_{k|k-1}$. The update step for the kinematic state x_k in (11a) and (11b) is given as a Kalman-filter-like update. The extent state update in (11c) and (11d) requires two new matrices

$$\hat{N} = \hat{X}^{1/2} S^{-1/2} \varepsilon\varepsilon^T S^{-T/2} \hat{X}^{T/2}, \tag{12a}$$

$$\hat{Z} = \hat{X}^{1/2} \hat{R}^{-1/2} \Sigma_{\breve{Z}_k} \hat{R}^{-T/2} \hat{X}^{T/2}, \tag{12b}$$

which are proportional to, respectively, the spread of the predicted measurement $\varepsilon\varepsilon^T$ and the converted sample spread $\Sigma_{\breve{Z}_k}$. We can further apply the converted measurement statistics to other random matrix-based state update steps [23, 24].

4.3. Truncation Bound Update

The final step is to update the truncation bounds, given the above updated state $\xi_{k|k}$. Due to space limitations, we only briefly outline the steps necessary for updating truncation bounds. The idea is to maximize the joint measurement likelihood

$$p(Z_k|\xi)|_{\xi_k = \xi_{k|k}} = \prod_j p(z_k^j|\xi_k)_{\xi = \xi_{k|k}} \tag{13}$$

over $B_k \triangleq [a_{k,1}, a_{k,2}, b_{k,1}, b_{k,2}]^T$, where the spatial distribution $p(z_k^j|\xi_k)$ is given by (4) with ξ_k replaced by the updated state $\xi_{k|k}$ and, thus, is a function of B_k viz the normalization factor c_{D_k} and the integral in (4).

We first convert the measurements in the global coordinate to the object local coordinate such that the orientation of the truncated area (specified by D_k) is aligned with the axes. Thus we can decouple the expression of the measurement likelihood $p(Z_k|\xi_k)$ as a function of four truncation bounds B_k via the cumulative density function of a standard normal distribution. We then apply the coordinate ascent

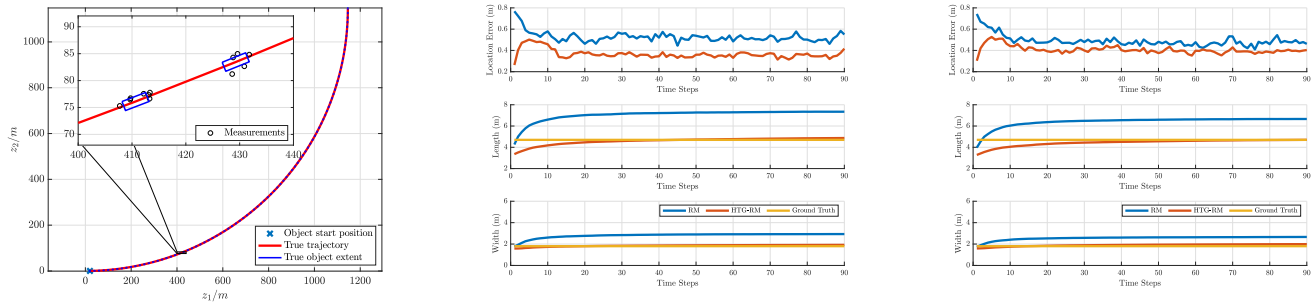

(a) (b) (c)

Fig. 4: (a) The simulated trajectory, object extent and sample measurements; and estimation results in terms of localization error, object's width and length estimations in (b) ideal measurement model and (c) with model mismatch.

to maximize the derived joint measurement likelihood along one direction at a time. More specifically, we cyclically find the optimal estimate of a single truncation bound at each iteration (e.g., using the Newton's method), while fixing the other three.

5. SIMULATION RESULTS

In this section, we consider a scenario in which a rectangular object (4.7-m long and 1.8-m wide) moves with constant polar velocity and turn rate for 90 time steps, as shown in Fig. 4(a). The number of measurements at each time step is drawn from a Poisson distribution with mean 8. We assume that the object rotation center coincides the object physical center. The kinematic object state is defined as $x_k = [p_k, v_k, \theta_k, \omega_k]^T \in \mathbb{R}^5$ with the two-dimensional position $p_k \in \mathbb{R}^2$, polar velocity v_k, heading θ_k and turn rate ω_k. The coordinated turn motion model is used with a sampling time of $T_s = 1s$ and standard polar and angular acceleration noise of $\sigma_{\dot{v}} = 0.1$ and $\sigma_{\dot{\omega}} = \pi/180$, respectively. The exact expressions for the transition matrix $g(\cdot)$ and process noise covariance matrix Q can be found in [25]. The transformation function E is a rotation matrix that depends on the turn rate. Given the posterior density of extent state $\mathcal{IW}(X_k; \nu_{k|k}, V_{k|k})$, the estimates of length l and width w can be extracted from the normalized eigen-decomposition of the mean of the inverse Wishart distribution, $\hat{X}_k = V_{k|k}/(\nu_{k|k} - 6)$; its initial parameters were set to $\nu_{0|0} = 22$ and $\nu_{0|0} = \text{diag}([40, 10])$.

5.1. Performance Evaluation with Ideal Measurement Model

We first consider the *ideal* case that the automotive radar measurements follow the proposed measurement model over the course of the simulated trajectory, with parameters specified in the caption of Fig. 2 and $R_k = \text{diag}([0.125, 0.125])$. Figure 4(a) shows two snapshots of synthesized automotive radar measurements around the object. It can be seen that most of these radar measurements appear to be around the object edges. We compare the tracking performance between the random matrix approach [19] (RM) and the proposed method (referred to as HTG-RM), averaged over 100 Monte Carlo runs. Fig. 4(b) shows the tracking performance in terms of localization errors (w.r.t object center), and object length/width errors over time. As evident, the proposed HTG-RM algorithm outperforms the conventional RM approach by a large margin in all aspects. Particularly, the HTG-RM algorithm provides more consistent estimates in terms of the object length and width over time. Corresponding root mean squared errors (RMSEs) of the kinematic and extent states are summarized in Table 1.

	Ideal Measurement Model		Model Mismatch	
States	RM	HTG-RM	RM	HTG-RM
p [m]	0.527	0.365	0.490	0.407
v [m]	0.097	0.062	0.096	0.064
θ [°]	0.879	0.723	0.835	0.799
l [m]	2.370	0.207	1.731	0.259
w [m]	1.007	0.081	0.758	0.127

Table 1: Root mean square errors of the estimated state parameters

5.2. Performance Evaluation with Model Mismatch

In practice, no measurement models can perfectly describe the real-world automotive radar measurements. To validate the effectiveness of the proposed HTG-RM algorithm in case of model mismatch, we adopt a variational radar model of 50 student's t mixture components, learned offline from aggregated real-world automotive radar measurements [21], to synthesize the observed radar measurement over the course of Fig. 4(a). It is worth noting that the resulting variational radar model in [21, Fig. 4] also shows a high probability of measurement occurrence around the object edge with a certain volume. It can be seen from Fig. 4(c) that the proposed HTG-RM algorithm still outperforms the conventional RM approach [19]. Compared to the ideal measurement model in Fig. 4(b), the HTG-RM performance is only slightly degraded, validating the robustness of the proposed HTG-RM algorithm over a different surface volume measurement model. This is further confirmed by comparing the root mean square errors of the kinematic and extent state estimates between the two columns of Table 1.

6. CONCLUSIONS

In this paper, we propose a new surface-volume measurement model for automotive radar object tracking, using a hierarchical truncated Gaussian model. The proposed measurement model has been integrated into the random matrix approach for extended object tracking using pseudo measurements and the resulting converted measurement statistics. Our simulations validate and demonstrate the effectiveness of our approach.

7. REFERENCES

[1] K. Gilholm, S. Godsill, S. Maskell, and D. Salmond, "Poisson models for extended target and group tracking," in *Signal and Data Processing of Small Targets*. 2005, vol. 5913, pp. 230 – 241, SPIE.

[2] K. Gilholm and D. Salmond, "Spatial distribution model for tracking extended objects," *IEE Proceedings - Radar, Sonar and Navigation*, vol. 152, pp. 364–371(7), October 2005.

[3] J. Degerman, J. Wintenby, and D. Svensson, "Extended target tracking using principal components," in *14th International Conference on Information Fusion*, July 2011, pp. 1–8.

[4] J. Lan and X. R. Li, "Tracking of extended object or target group using random matrix — Part I: New model and approach," in *2012 15th International Conference on Information Fusion*, July 2012, pp. 2177–2184.

[5] D. Angelova, L. Mihaylova, N. Petrov, and A. Gning, "A convolution particle filtering approach for tracking elliptical extended objects," in *Proceedings of the 16th International Conference on Information Fusion*, July 2013, pp. 1542–1549.

[6] J. Lan and X. R. Li, "Tracking of extended object or target group using random matrix: new model and approach," *IEEE Trans. on Aerospace and Electronic Systems*, vol. 52, no. 6, pp. 2973–2989, December 2016.

[7] K. Granström, M. Baum, and S. Reuter, "Extended object tracking: Introduction, overview, and applications," *Journal of Advances in Information Fusion*, vol. 12, no. 2, 2017.

[8] S. Yang and M. Baum, "Tracking the orientation and axes lengths of an elliptical extended object," *IEEE Trans. on Signal Processing*, vol. 67, no. 18, pp. 4720–4729, Sep. 2019.

[9] M. Buhren and B. Yang, "Simulation of automotive radar target lists using a novel approach of object representation," in *2006 IEEE Intelligent Vehicles Symposium*, June 2006, pp. 314–319.

[10] J. Gunnarsson, L. Svensson, L. Danielsson, and F. Bengtsson, "Tracking vehicles using radar detections," in *2007 IEEE Intelligent Vehicles Symposium*, June 2007, pp. 296–302.

[11] L. Hammarstrand, M. Lundgren, and L. Svensson, "Adaptive radar sensor model for tracking structured extended objects," *IEEE Trans. on Aerospace and Electronic Systems*, vol. 48, no. 3, pp. 1975–1995, JULY 2012.

[12] M. Baum and U. D. Hanebeck, "Random hypersurface models for extended object tracking," in *2009 IEEE International Symposium on Signal Processing and Information Technology (ISSPIT)*, 2009, pp. 178–183.

[13] M. Baum and U. D. Hanebeck, "Extended object tracking with random hypersurface models," *IEEE Trans. on Aerospace and Electronic Systems*, vol. 50, no. 1, pp. 149–159, 2014.

[14] P. Broßeit, M. Rapp, N. Appenrodt, and J. Dickmann, "Probabilistic rectangular-shape estimation for extended object tracking," in *2016 IEEE Intelligent Vehicles Symposium (IV)*, June 2016, pp. 279–285.

[15] X. Cao, J. Lan, X. R. Li, and Y. Liu, "Extended object tracking using automotive radar," in *2018 21st International Conference on Information Fusion (FUSION)*, July 2018, pp. 1–5.

[16] N. Wahlström and E. Özkan, "Extended target tracking using Gaussian processes," *IEEE Trans. on Signal Processing*, vol. 63, no. 16, pp. 4165–4178, 2015.

[17] K. Thormann, M. Baum, and J. Honer, "Extended target tracking using Gaussian processes with high-resolution automotive radar," in *2018 21st International Conference on Information Fusion (FUSION)*, July 2018, pp. 1764–1770.

[18] J. W. Koch, "Bayesian approach to extended object and cluster tracking using random matrices," *IEEE Trans. on Aerospace and Electronic Systems*, vol. 44, no. 3, pp. 1042–1059, July 2008.

[19] M. Feldmann, D. Frnken, and W. Koch, "Tracking of extended objects and group targets using random matrices," *IEEE Transactions on Signal Processing*, vol. 59, no. 4, pp. 1409–1420, April 2011.

[20] P. Broßeit, B. Duraisamy, and J. Dickmann, "The volcanormal density for radar-based extended target tracking," in *2017 IEEE 20th International Conference on Intelligent Transportation Systems (ITSC)*, Oct 2017, pp. 1–6.

[21] A. Scheel and K. Dietmayer, "Tracking multiple vehicles using a variational radar model," *IEEE Trans. on Intelligent Transportation Systems*, vol. 20, no. 10, pp. 3721–3736, Oct 2019.

[22] K. Granström and U. Orguner, "New prediction for extended targets with random matrices," *IEEE Trans. on Aerospace and Electronic Systems*, vol. 50, no. 2, pp. 1577–1589, 2014.

[23] U. Orguner, "A variational measurement update for extended target tracking with random matrices," *IEEE Trans. on Signal Processing*, vol. 60, no. 7, pp. 3827–3834, 2012.

[24] K. Granström, A. Natale, P. Braca, G. Ludeno, and F. Serafino, "Gamma Gaussian inverse Wishart probability hypothesis density for extended target tracking using X-band marine radar data," *IEEE Trans. on Geoscience and Remote Sensing*, vol. 53, no. 12, pp. 6617–6631, 2015.

[25] X.R. Li and V. P. Jilkov, "Survey of maneuvering target tracking. Part I. dynamic models," *IEEE Trans. on Aerospace and Electronic systems*, vol. 39, no. 4, pp. 1333–1364, 2003.